Available online at www.sciencedirect.com
ScienceDirect
Dyes and Pigments 77 (2008) 43–47
DYES and PIGMENTS
www.elsevier.com/locate/dyepig

The synthesis, characterization and photocatalytic activity of V(V), Pb(II), Ag(I) and Co(II)-doped Bi_2O_3

Jimin Xie*, Xiaomeng Lü, Min Chen, Ganqing Zhao, Yuanzhi Song, Shuaishuai Lu

School of Chemistry and Chemical Engineering, Jiangsu University, Zhenjiang 212013, PR China

Received 13 December 2006; accepted 25 February 2007
Available online 12 March 2007

Abstract

Bi_2O_3 samples doped with several transition metal ions ($M-Bi_2O_3$, where $M = V^V$, Pb^{II}, Ag^I and Co^{II}) were synthesized using a precipitation method in the presence of sodium dodecyl benzene sulphonate (SDBS). The compounds were characterized by X-ray diffraction (XRD), scanning electron microscopy (SEM), transmission electron microscopy (TEM), UV–visible diffuse reflection spectroscopy (UV–vis DRS) and photoluminescence (PL). The monoclinic microcrystal samples displayed different morphology and visible-light harvesting character. The photocatalytic activity of the $M-Bi_2O_3$ compounds, evaluated by the extent of decolorization of *Rhodamine B* under visible light, followed the order: $V(V)-Bi_2O_3 > Pb(II)-Bi_2O_3 > Ag(I)-Bi_2O_3 > Co(II)-Bi_2O_3 >$ undoped Bi_2O_3.

Keywords: Synthesis; Spectroscopy; Doped; Bi_2O_3; Photodecolorization; Photoluminescence

1. Introduction

Visible-light-driven photocatalysts have attracted interest in recent years because visible light is an important clean energy and can be easily utilized. In order to use solar energy efficiently, the key step is to explore new materials as visible-light-driven photocatalysts [1–5]. It was reported that modified TiO_2 [6–11], complex oxides such as $CaBi_2O_4$ [12], $InMO_4$ (M = Nb, Ta, V) [13] and $PbBi_2Nb_2O_9$ [14] function as visible-light-driven photocatalysts.

Bismuth oxide is an important metal-oxide semiconductor and can be used to decompose Orange II in water [9]. Compared to conventional techniques, Bi_2O_3 synthesized by precipitation method is of high purity, high activity and narrow particle size distribution [15]. However, the structure (crystalline size and shape, phase composition, presence of amorphous phase, etc.) of Bi_2O_3 depends on the preparation conditions [16]. In this work, precursors of Bi_2O_3 and $M-Bi_2O_3$ ($M = V^V$, Pb^{II}, Ag^I and Co^{II}) were synthesized by a precipitation method and the effect of the different metal ions on the photocatalytic degradation of *Rhodamine B* under visible light by Bi_2O_3 was determined.

2. Experimental

2.1. Preparation of catalysts

All chemicals were of analytical grade and were used without further purification. Bi_2O_3 was prepared by adding 1 mol/L of aq. NaOH solution to a solution of $Bi(NO_3)_3$ and SDBS (0.1 mol/L) with continuous stirring. The precipitate obtained was filtrated, washed with water and then dried and calcined at 500 °C for 2 h. $M-Bi_2O_3$ samples were prepared by adding $M(NO_3)_x$ to $Bi(NO_3)_3$ solution in the mole ratio, M:Bi=1:200 with SDBS (0.1 mol/L) as surfactant. The pH of the ensuing solution was adjusted to 12 by the addition of 1 mol/L aq. NaOH solution at 40 °C. The resulted emulsion was filtered and the residue was washed in de-ionized water and ethanol, respectively, before being dried and calcined at 500 °C for 2 h.

* Corresponding author. Fax: +86 511 8791708.
E-mail address: xiejm391@sohu.com (J. Xie).

0143-7208/$ - see front matter © 2007 Elsevier Ltd. All rights reserved.
doi:10.1016/j.dyepig.2007.02.011

2.2. Characterization of catalysts

Bi_2O_3 and M–Bi_2O_3 were characterized by powder X-ray diffraction (XRD) using a D/max-γA X-ray diffractometer at 40 kV and 200 mA with monochromatic Cu Kα ($\lambda = 1.5418$ Å) radiation. Diffraction patterns of the powder samples held on quartz zero background plates were obtained using θ–θ geometry. Morphologies were further examined using a Phillips *XL-30* scanning electron microscope at an accelerating voltage of 20 kV. Transmission electron microscopy (TEM) images were taken on a Phillips *TECNAI12* instrument. UV–vis diffuse reflectance spectra (DRS) were recorded on a Shimadzu *UV-2401* spectrophotometer equipped with spherical diffuse reflectance accessory and photoluminescence spectra (FL) were obtained using a Cary *Eclipse* scanning UV–vis system.

2.3. Measurement of the photodecolorization activity

The photocatalytic efficiency of Bi_2O_3 and M–Bi_2O_3 was investigated by the extent of decolorization of *Rhodamine B* under visible irradiation using a blended-light mercury fluorescent lamp ($\lambda \geq 410$ nm). Bi_2O_3 or M–Bi_2O_3 (100 mg) was added to 100 mL of an aq. *Rhodamine B* (10 mg/L) solution, which was kept in the dark for 1 h before irradiation. At given time intervals, a 5 mL aliquot was analyzed at 554 nm using a Shimadzu *UV-2450* spectrophotometer.

3. Results and discussion

3.1. Structure analysis

It has been reported that Bi_2O_3 has four different polymorphic forms, several non-stoichiometric forms as well as impure phases [17]. In general, the polymorphic form depends on the employed synthetic method. In this work, the diffraction lines of Bi_2O_3 implied that the sample sintered at 500 °C was monoclinic form according to JCPDS file no. 41-1449. The XRD patterns of samples which had been doped with different transition metal ions displayed similar diffraction lines and high crystallinity. The presence of separate oxide phases was not observed, possibly due to the low dopant concentration used or the substitution of Bi^{3+} lattice sites by the doped metal ions. The UV–vis spectra of nanocrystallite Bi_2O_3 and M–Bi_2O_3 revealed that all samples could absorb light up to the visible region. The V(V)–Bi_2O_3 had a broad intense absorption peak at 350 nm (Fig. 1). It is well known that the color of a solid depends on the position of its absorption edge, which is related to the frequency (ν) of the absorbed light and the band gap (E_g) as shown in Eq. (1) [18]

$$A = \frac{C\left(h\nu - E_g\right)^{1/2}}{h\nu} \tag{1}$$

where A is the absorption coefficient, h Plank's constant and C a constant. On a plot of $(A \times h\nu)^2$ as a function of $(h\nu)$, a linear relationship should be seen in the vicinity of the absorption edge and the forbidden band gap (E_g) can be estimated from the intercept. Thus, the band gap E_g of Bi_2O_3 and V(V)–Bi_2O_3 was estimated to be 2.8 eV and 2.69 eV (Fig. 2), respectively.

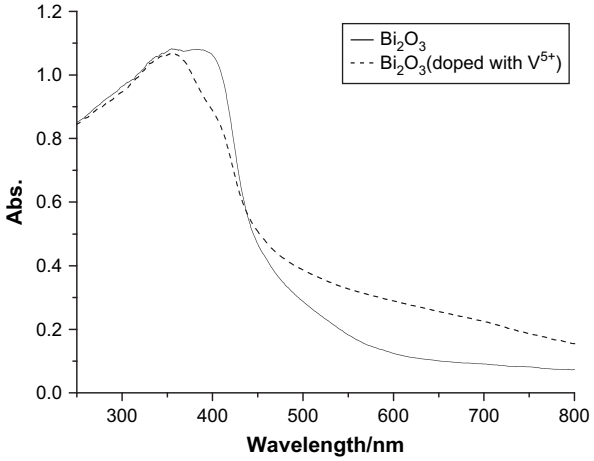

Fig. 1. UV–vis spectra of Bi_2O_3 and Bi_2O_3 (doped with V(V)).

The SEM images of M–Bi_2O_3 and Bi_2O_3 are shown in Fig. 3. It is apparent that Bi_2O_3 had a flake structure (Fig. 3d) and a rod shape was observed for V(V), Pb(II) and the Ag(I) doped Bi_2O_3 compounds (Fig. 3a–c). The average length of the M–Bi_2O_3 particles was 6.4 μm for V(V), 2.2 μm for Pb(II) and 5.3 μm for Ag(I), while the average thickness was 1.0 μm for V(V), 0.32 μm for Pb(II), and 1.1 μm for Ag(I).

The TEM images of Bi_2O_3 and V(V)–Bi_2O_3 are shown in Fig. 4. The Bi_2O_3 crystallites were cubical in shape (Fig. 4a); it is evident that agglomeration occurred as a result of the sintering process. In the case of V(V)–Bi_2O_3, the particles were smaller in size and exhibited a quite uniform structure (Fig. 4b).

Photoluminescence emission spectra are often used to examine the efficiency of charge carrier trapping, immigration and transfer, as well as understand the fate of e^-/h^+ pairs in semiconductor particles [19]. The photoluminescence emission spectra of Bi_2O_3 and M–Bi_2O_3 are shown in Fig. 5.

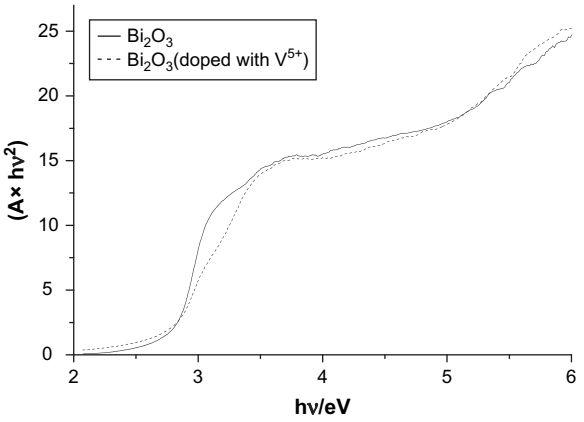

Fig. 2. Graph of samples plotted as $(A \times h\nu)^2$ vs $(h\nu)$.

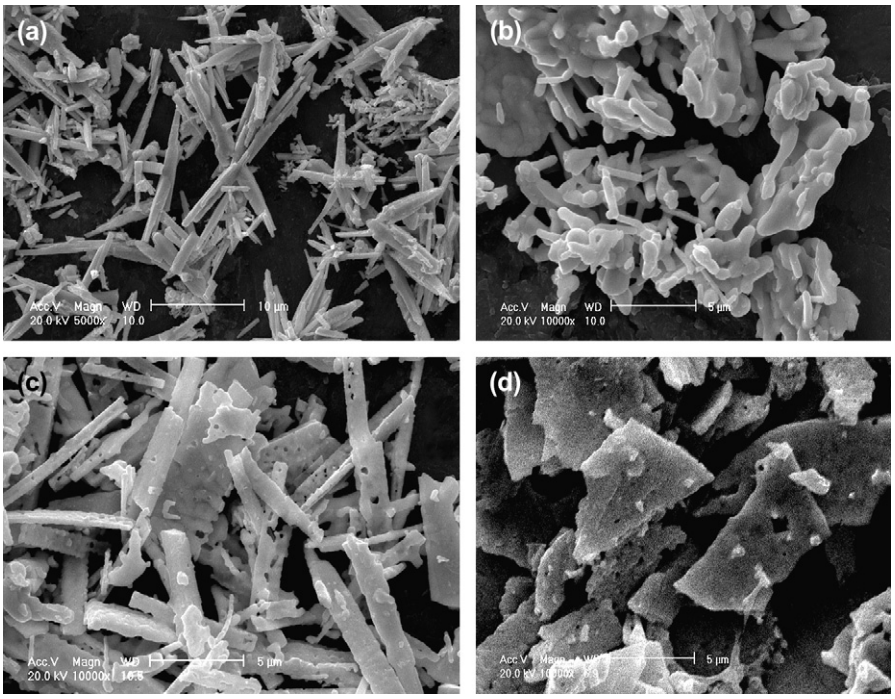

Fig. 3. SEM images of Bi_2O_3 doped with V (a), Pb (b), Ag (c) and pure Bi_2O_3 (d).

Though identical shapes and peak positions (~116 nm) were observed, the emission band intensities of the spectra varied for the different metal ions used. The highest band intensity was recorded for Bi_2O_3 and the lowest for V(V)–Bi_2O_3 (Fig. 5). The photoluminescence intensities of M–Bi_2O_3 were 88.03 (Co^{2+}), 86.30 (Ag^{+}), 80.26 (Pb^{2+}) and 63.91 (V^{5+}). It is known that the photoluminescence spectrum of Bi_2O_3 can be attributed to the radiative recombination process of self-trapped excitations [15]. Therefore, the observed lower intensity for M-doped Bi_2O_3 indicates that radiative recombination was lowered by doping with the transition metal ions, leading to weak recombination of the e^{-}/h^{+} pairs and high photon efficiency. Hence, the results suggest that the V(V)-doped Bi_2O_3 had highest photo-efficiency of all the samples examined in this work and could be used as an effective photocatalyst.

3.2. The photocatalytic degradation of Rhodamine B

After sensitized ''internally'' by doping with transition metal ions, such as Co(II), Ag(I), Pb(II) or V(V) and ''externally'' by employing photo-sensitizers such as *Rhodamine B*, Bi_2O_3 can be a good light-absorbing catalyst. As an example, the spectral changes obtained during the photodecoloration of *Rhodamine B* catalyzed by Ag(I)–Bi_2O_3 are shown in Fig. 6. The initial *Rhodamine B* displayed a major absorption band at 553 nm. However, the intensity of this band was halved and the band was shifted 14 nm to 539 nm after 180 min

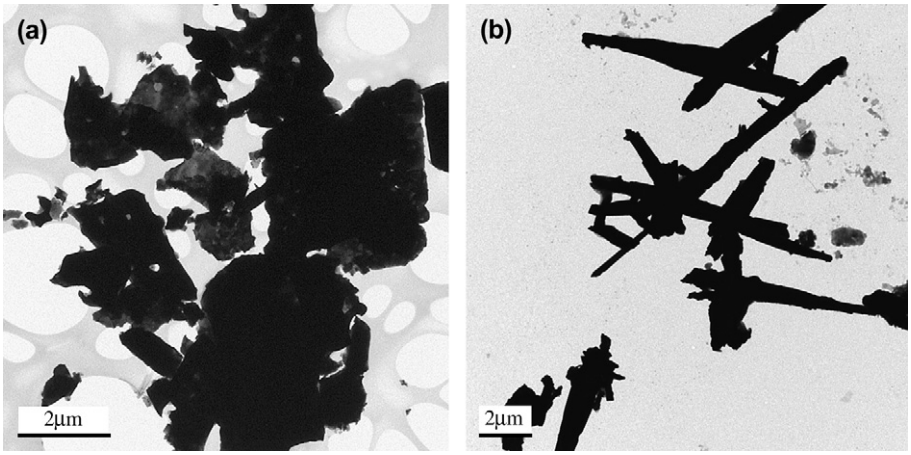

Fig. 4. TEM spectra of Bi_2O_3 (a) and Bi_2O_3 doped with V (b).

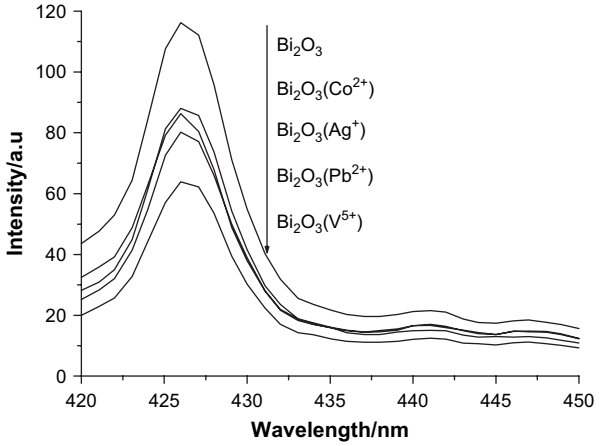

Fig. 5. Photoluminescence (PL) spectra: comparison of Bi_2O_3 and the samples of Bi_2O_3 doped with Co^{2+}, Ag^{+}, Pb^{2+}, and V^{5+}.

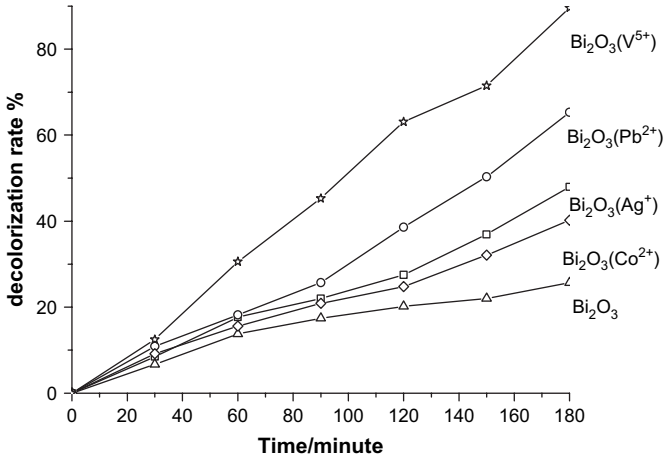

Fig. 7. Effect of the photodecolorization activity of *Rhodamine B* using Bi_2O_3 samples.

irradiation, indicating that degradation of *Rhodamine B* occurred and led to the formation of *N*,*N*,*N*′-triethyl *Rhodamine* [20]. In the case of Bi_2O_3, the observed blue shift was only 4 nm (from 553 nm to 549 nm) under the same experimental conditions. These findings confirmed that the M−Bi_2O_3 samples have higher photocatalytic activity than Bi_2O_3.

The photodecolorization efficiencies of Bi_2O_3 and M−Bi_2O_3 are shown in Fig. 7. It has been reported that TiO_2 is inactive under visible light [21]. Whilst decolorization efficiency was 25.7% after 180 min irradiation using Bi_2O_3 as photocatalyst, in the cases of Co(II) and Ag(I) doped catalysts, the extent of degradation of *Rhodamine B* increased to 40% and 48%, respectively and in the case of Pb(II) and V(V)-doped catalytst, it was 65% and 89%, respectively. Thus, the M−Bi_2O_3 compounds have higher photodecolorization efficiency than Bi_2O_3 and followed the order: V(V)−Bi_2O_3 > Pb(II)−Bi_2O_3 > Ag(I)−Bi_2O_3 > Co(II)−Bi_2O_3. The different photocatalytic activities of the metal ions can be explained in terms of ionic radius, i.e., the ionic radius of V^{5+} (0.59 Å) is lower than that of the other metal ions (Bi^{3+} 0.96 Å, Ag^{+} 1.26 Å, Pb^{2+} 1.20 Å) therefore, the V^{5+} ions may more easily penetrate the Bi_2O_3 lattice, resulting in greater coverage of the Bi_2O_3 surface with vanadium oxide. The low photodecolorization activity of Co^{II}-doped Bi_2O_3 may be due to it behaving as an electron−hole recombination center (Fig. 5) because of its irregular morphology.

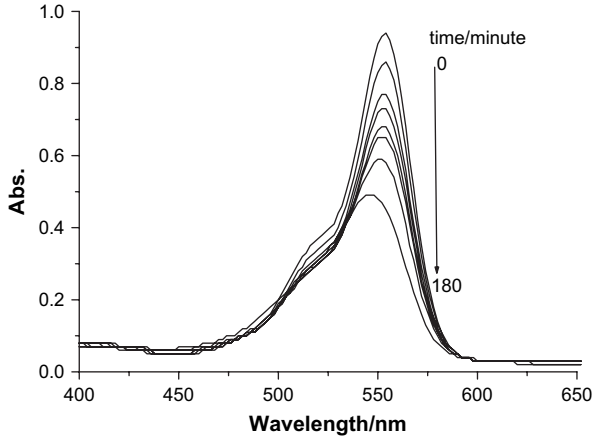

Fig. 6. Absorption changes of *Rhodamine B* photodecolorization process using Bi_2O_3 sample doped with Ag^{+}.

4. Conclusions

Both Bi_2O_3 and Bi_2O_3 samples doped with transition metal ions (i.e. M−Bi_2O_3 where M = V^{V}, Pb^{II}, Ag^{I} and Co^{II}) were synthesized by a precipitation method. While XRD showed that there were no changes in the structure and crystallinity of the catalyst as a result of doping with the metal ions, doping imparted distinct morphological and light absorption differences. All of the M−Bi_2O_3 compounds showed higher photodecolorization activity than undoped Bi_2O_3 under visible light ($\lambda \geq 410$ nm); in particular, V(V)−Bi_2O_3, exhibited significant photo-activity which implies that this particular compound may function as an efficient photocatalyst for the decolorization of organic pollutants.

Acknowledgments

This work was financially supported by Jiangsu Academic Leader Foundation (No. 2001013) and Jiangsu Social Development Foundation (No. BS2006038), PR China.

References

[1] Li D, Haneda H. Synthesis of nitrogen-containing ZnO powders by spray pyrolysis and their visible-light photocatalysis in gas-phase acetaldehyde decomposition. J Photochem Photobiol A Chem 2003;155(1−3):171−8.
[2] Wang J, Uma S, Klabunde KJ. Visible light photocatalysis in transition metal incorporated titania−silica aerogels. Appl Catal B Environ 2004;48(2):151−4.
[3] Martyanov IN, Uma S, Rodrigues S, Klabunde KJ. Structural defects cause TiO2-based photocatalysts to be active in visible light. Chem Commun 2004;2476−7.
[4] Li D, Haneda H. Photocatalysis of sprayed nitrogen-containing Fe_2O_3−ZnO and WO_3−ZnO composite powders in gas-phase acetaldehyde decomposition. J Photochem Photobiol A Chem 2003;160(3):203−12.

[5] Anpo M, Takeuchi M. The design and development of highly reactive titanium oxide photocatalysts operating under visible light irradiation. J Catal 2003;216(1–2):505–16.
[6] Zhang L, Lin J, Chen Z, Tang Y, Yu Y. Preparation of Fenton reagent with H_2O_2 generated by solar light-illuminated nano-Cu_2O/MWNTs composites. Appl Catal A Gen 2006;299:292–7.
[7] Maruthamuthu P, Gurunathan K, Subramanian E, Sastri MVC. Visible light-induced hydrogen production from water with $Pt/Bi_2O_3/RuO_2$ in presence of electron relay and photosensitizer. Int J Hydrogen Energy 1994;19(11):889–93.
[8] Gurunathan K. Photocatalytic hydrogen production using transition metal ions-doped γ-Bi_2O_3 semiconductor particles. Int J Hydrogen Energy 2004;29(9):933–40.
[9] Bessekhouad Y, Robert D, Weber JV. Photocatalytic activity of Cu_2O/TiO_2, Bi_2O_3/TiO_2 and $ZnMn_2O_4/TiO_2$ heterojunctions. Catal Today 2005;101(3–4):315–21.
[10] Mdleleni MM, Hyeon T, Suslick KS. Sonochemical synthesis of nanostructured molybdenum sulfide. J Am Chem Soc 1998;120:6189–90.
[11] Dhas NA, Suslick KS. Sonochemical preparation of hollow nanospheres and hollow nanocrystals. J Am Chem Soc 2005;127:2368–9.
[12] Tang J, Zou Z, Ye J. Efficient photocatalytic decomposition of organic contaminants over $CaBi_2O_4$ under visible light irradiation. Angew Chem Int Ed 2004;43:4463–6.
[13] Ye J, Zou Z, Arakawa H, Oshikiri M, Shimoda M, Matsushita A, et al. Correlation of crystal and electronic structures with photophysical properties of water splitting photocatalysts $InMO_4$ ($M = V^{5+}$, Nb^{5+}, Ta^{5+}). J Photochem Photobiol A Chem 2002;148(1–3):79–83.
[14] Kim HG, Hwang DW, Lee JS. An undoped, single-phase oxide photocatalyst working under visible light. J Am Chem Soc 2004;126:8912–3.
[15] Li W. Preparation of monodisperse nanometer Bi_2O_3 powder. J Cent South Univ Technol 2005;36(2):175–8.
[16] Leontie L, Caraman M, Delibas M. Optical properties of bismuth trioxide thin films. Mater Res Bull 2001;36(9):1629–37.
[17] Medernach JW, Snyder RL. Powder diffraction patterns and structures of the bismuth oxides. J Am Ceram Soc 1978;61(11):494–7.
[18] Fu H, Pan C, Yao W, Zhu Y. Visible-light-induced degradation of rhodamine B by nanosized Bi_2WO_6. J Phys Chem B 2005;109:22432–9.
[19] Yu JG, Yu HG, Cheng B, Zhao XJ, Yu JC, Ho W-K. The effect of calcination temperature on the surface microstructure and photocatalytic activity of TiO_2 thin films prepared by liquid phase deposition. J Phys Chem B 2003;107:13871–9.
[20] Asahi R, Morikawa T, Ohwaki T, Aoki K, Taga Y. Photocatalysts sensitive to visible light. Science 2001;293:269–71.
[21] Zhang C, Zhu Y. Synthesis of square Bi_2WO_6 nanoplates as high-activity visible-light-driven photocatalysts. Chem Mater 2005;17:3537–45.